UDC 624.04

ANALYSIS ON THERMAL STRESS OF ULTRA-LONG BASEMENT BASED ON XFEM AND STRESS TRAJECTORY VISUALIZATION

Hongyang Xie[1], Yuhang Ren[2], Hao Zheng[3], A. E. Zheltkovich[4], Wei Fu[5], Zhuoyu Min[6], Meixin Shuai[7], Yiwen Dai[8]

[1] Candidate of Technical Sciences, Professor, College of Civil Engineering and Architecture, Nanchang Hangkong University, Nanchang, China, e-mail: xiehongyang486@163.com
[2] Master's student, Belarusian national technical university and Nanchang Hangkong University, Minsk, Belarus, e-mail: reny23312@gmail.com
[3] Master's student, Nanchang Hangkong University, Nanchang, China, e-mail: 1486197683@qq.com
[4] Candidate of Technical Sciences, Associate Professor, Department of Applied Mechanics, Brest State Technical University, Brest, Belarus, e-mail: gelpek@mail.ru
[5] Master's student, Nanchang Hangkong University, Nanchang, China, e-mail: 987327843@qq.com
[6] Master's student, Nanchang Hangkong University, Nanchang, China, e-mail: 343791215@qq.com
[7] Master's degree, Associate professor, College of Civil Engineering and Architecture, Nanchang Hangkong University, Nanchang, China, e-mail: 358298863@qq.com
[8] Master's student, Nanchang Hangkong University, Nanchang, China, e-mail: dyw2458751868@163.com

Abstract

Research is conducted on the cracking problem of the side walls of ultra-long seamless basement structures under high-temperature and sunny construction environments in summer. Long term temperature monitoring was conducted on a basement under construction in the Modern Service Industry Park of Honggutan District, Nanchang City. The temperature field was simulated using the commercial finite element software Abaqus, and the measured results were compared with the simulation results to verify the rationality of the theory of simulating the temperature field of sunlight. Based on the theory of simulating the temperature field of sunlight, numerical simulation experiments were conducted using the Extended Finite Element Method (XFEM) to analyze the temperature and stress fields of complete basement structures of different lengths in high-temperature sunlight environments. The differences in stress and critical cracking temperature difference of basement side walls of different lengths under the same temperature field were compared. Abaqus software was redeveloped using a principal stress trajectory visualization program written in Python, and a complete principal stress trajectory diagram of the basement structure was drawn. The analysis results show that under the same temperature gradient, the change in basement length has no significant effect on the magnitude of the principal stress on the side walls. The critical temperature difference between the upper and lower parts of the basement that caused the side wall to crack did not change significantly. Under the effect of uneven expansion, the crack shape of the basement side wall is in the shape of a "八". In high-temperature construction environments, the temperature rise of the basement ceiling should be carefully monitored to avoid excessive temperature differences between the upper and lower parts of the structure, which may cause the side walls to crack.

Keywords: reinforced concrete basement, sunshine temperature field, crack control, extended finite element method, principal stress trajectory, post-cast strip.

АНАЛИЗ ТЕРМИЧЕСКОГО НАПРЯЖЕНИЯ УЛЬТРАДЛИННОГО ПОДЗЕМНОГО СООРУЖЕНИЯ НА ОСНОВЕ XFEM И ВИЗУАЛИЗАЦИИ ТРАЕКТОРИИ НАПРЯЖЕНИЙ

Хунъян Се, Юйхан Жэнь, Хао Чжэн, А. Е. Желткович, Вэй Фу, Чжоюй Мин, Мэйсинь Шуай, Ивэнь Дай

Реферат

Исследуется проблема растрескивания боковых стен ультрадлинных бесшовных подземных конструкций в условиях высокой температуры и солнечного освещения летом. Долгосрочный мониторинг температуры проводился на подземном сооружении, строящемся в Современном сервисном индустриальном парке района Хунгутан города Нанчанг. Температурное поле моделировалось с использованием коммерческого программного обеспечения конечных элементов Abaqus, а измеренные результаты сравнивались с результатами моделирования для проверки обоснованности теории моделирования температурного поля солнечного света. На основе теории моделирования температурного поля солнечного света были проведены численные симуляционные эксперименты с использованием Расширенного метода конечных элементов (XFEM) для анализа температурных и напряженных полей полноразмерных подземных конструкций различной длины в условиях высокой температуры солнечного света. Сравнивались различия в напряжении и критическая температура растрескивания боковых стен подземных сооружений различной длины при одном и том же температурном поле. Программное обеспечение Abaqus было дополнительно разработано с использованием программы визуализации траектории главных напряжений, написанной на Python, и был составлен полный диаграмма траектории главных напряжений подземного сооружения. Результаты анализа показывают, что при одинаковом температурном градиенте изменение длины подземного сооружения не оказывает значительного влияния на величину главного напряжения на боковых стенах. Критическая температура между верхней и нижней частями подземного сооружения, вызывающая растрескивание боковых стен, не изменялась значительно. Под действием неравномерного расширения форма трещины боковой стены подземного сооружения принимает вид «八». В условиях высокой температуры строительства необходимо тщательно контролировать повышение температуры потолка подземного сооружения, чтобы избежать чрезмерных температурных различий между верхней и нижней частями конструкции, что может вызвать растрескивание боковых стен.

Ключевые слова: железобетонное подземное сооружение, температурное поле солнечного света, контроль трещин, расширенный метод конечных элементов, траектория главного напряжения, постформировочная лента.

Introduction

Due to its excellent ability to utilize urban space, the structural form of "upper high-rise buildings + large area basements" has become the mainstream form of urban space development in China today. Especially the ultra-long seamless basement structure, due to its good overall integrity, ability to shorten construction period and improve engineering efficiency, is increasingly being applied in engineering [1]. Along with it comes the serious problem of crack control. Cracks on the exterior walls of the basement can cause problems such as water leakage, steel corrosion, and difficulty in repair, which in turn affect the durability and safety of the overall structure. In the past, the mainstream research on this topic both domestically and internationally was focused on the early hydration heat and temperature shrinkage of concrete [2–8]. In recent years, research on the temperature field of various concrete structures under sunlight has become increasingly common. Zhang Hanshuo et al. conducted long-term temperature field monitoring on the ultra-long concrete structure of the newly built station building at Xiamen North Railway Station. Their method of considering both the early hydration heat release of concrete and the influence of sunlight radiation in the thermal mechanical coupling finite element simulation provides a reference for related research [9]. The same numerical simulation theory of sunshine temperature field is also applicable to the analysis of structures such as concrete beam bridges, hydraulic concrete structures, and concrete basements [10, 11].

Long term engineering practice has shown that the cracking problem of basement structural side walls during summer construction is particularly severe in the vast southern regions of China. The basement structure constructed in a high-temperature sunlight environment can reach a surface temperature of over 60 degrees Celsius due to the long-term exposure of the roof to direct sunlight after demoulding and before backfilling the foundation pit. The bottom plate is located on the soil and is not affected by sunlight, resulting in a lower temperature. Under the influence of a large temperature gradient between the upper and lower parts of the structure, there will be significant differences in thermal expansion deformation. The upper part of the basement has a large amount of thermal expansion deformation, while the lower part has a small amount of thermal expansion, and the side walls are easily torn. This is the phenomenon of side wall cracking caused by the uneven expansion effect of the structure, and there is currently no relevant research on this aspect. Considering the differences between the problem of uneven expansion of concrete basements under temperature gradient and other temperature effects, there are two issues worth further discussion:

1. Will uneven expansion effect lead to cracking of side walls? There are many factors that affect the cracking of ultra-long basement structures, and the mechanism of uneven expansion effect induced cracking is not yet clear. There is still insufficient research on the differences in cracking morphology compared to other types of cracking.

2. The quantitative relationship between the magnitude of thermal stress generated by the temperature gradient between the upper and lower parts of the structure and the length of the basement is not yet clear.

In response to the above two issues, this article first conducts long-term temperature field monitoring of a basement project under construction in Nanchang City, Jiangxi Province, and uses concrete sunlight temperature field simulation theory to finely model and analyze the structure. The comparison between simulated data and measured results verified the rationality of the simulation theory. Then, based on this theory, the powerful function of the extended finite element method (XFEM) in simulating discontinuous problems such as interface development and crack growth is utilized for parameter analysis, and the crack morphology of the sidewall is predicted [12]. And the Abaqus software was further developed using a Python script editing program to draw the principal stress trajectory diagram of complete basement structure. Identify the cracking morphology and mechanism of basement side walls under the effect of uneven expansion. To investigate the quantitative relationship between the length of the basement and the critical temperature difference between the upper and lower parts that causes side wall cracking, in order to adopt different degrees of temperature control measures for basements of different lengths, and provide theoretical reference for similar crack control problems in practical engineering.

1 Simulation theory of concrete sunshine temperature field

There are three main ways of heat transfer in basement structures under sunlight conditions: heat conduction, heat convection, and heat radiation [13, 14, 15].

1.1 Heat conduction simulation

Heat conduction refers to the transfer of heat from the higher temperature parts of concrete to the lower temperature parts, and is the main way of heat transfer in solids, defined in the Abaqus material properties. According to Fourier's law $q_x'' = -k\frac{dT}{dx}$, under a constant temperature gradient, the heat transfer rate is proportional to the thermal conductivity of the material. Liu Xingfa et al. found that the range of thermal conductivity values for concrete materials is 1.16~3.5J/(m·s·K) [14]. The value obtained by Liu Cheng and others through thermal performance testing is 3.0J/(m·s·K) [16]. Article 4.1.8 of the "Code for Design of Concrete Structures" GB 50010-2010 states that when the temperature is within the range of 0 °C to 100 °C, the thermal conductivity of concrete can be set as 10.6kJ/(m·h·°C), which is 2.94J/(m·s·K) [17].

For the specific heat capacity of concrete, the range of values given in Appendix B.1 of the "Code for Thermal Design of Civil Building" GB 50176-2016 is 920~1050J/(kg·K) [18]. The recommended range of values given by Liu Xingfa and others after research is 879~1090J/(kg·K) [14].

1.2 Heat convection simulation

In the temperature field of concrete exposed to sunlight, convective heat transfer is the situation where the temperature of the concrete structure is driven by the increase in air temperature. Thermal convection simulation is defined in the Abaqus interaction module according to the "surface film condition". To define the thermal convection load conditions of concrete basement structures, it is necessary to measure or simulate the ambient temperature hourly. In the absence of hourly temperature monitoring data, the daily temperature model proposed by Liu Cheng et al. can be approximately used to simulate changes in external atmospheric temperature [16]. The specific calculation formula for environmental temperature $T_a(t)$ is shown in equation (1):

$$T_a(t)=\begin{cases}\dfrac{T_{\max}+T_{\min}}{2}-\dfrac{T_{\max}-T_{\min}}{2}\dfrac{t-t_{sr}+t_{night}}{t_{night}} & 0\le t\le t_{sr}\\ \dfrac{T_{\max}+T_{\min}}{2}-\dfrac{T_{\max}-T_{\min}}{2}\cos\left(\dfrac{3\pi}{2}\dfrac{t-t_{sr}}{t_{day}}\right) & t_{sr}\le t\le t_{ss}\\ T_{\max}-\dfrac{T_{\max}-T_{\min}}{2}\dfrac{t-t_{ss}+t_{night}}{t_{night}} & t_{ss}\le t\le 24\end{cases}. \quad (1)$$

In the formula: T_{max} is the highest daily temperature (°C); T_{min} is the daily minimum temperature (°C); t_{sr} is the sunrise time of the day (h); t_{ss} is the sunset time (h); t_{day} is the duration of daytime (h); t_{night} is the duration of nighttime (h).

1.3 Heat radiation simulation

The effect of solar radiation is one of the main factors causing the temperature rise of concrete structures. Solar radiation (shortwave radiation) can be divided into three categories: direct radiation, atmospheric scattering, and ground reflection, and its intensity is mainly affected by weather conditions such as atmospheric transparency.

https://doi.org/10.36773/1818-1112-2024-135-3-13-23

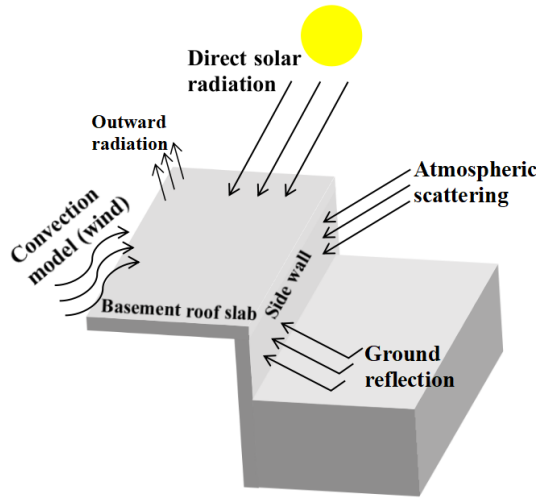

(a) Schematic diagram of sunlight radiation effect

(b) Cracks in the basement shear wall of Jinmei Hainan City project

Figure 1 – Schematic diagram of temperature field and high-temperature cracks in the basement (note: concrete was cast in June 2019, the highest daily temperature during the concrete curing period was 43 °C)

The direct radiation intensity on a plane perpendicular to the direction of solar radiation can be calculated using the following formula [10]

$$I_m = I_0 \frac{\sinh}{\sinh + \frac{1-P}{P}}. \quad (2)$$

In the formula: *h* is the solar altitude angle; *P* is the atmospheric transparency coefficient, which can be obtained by checking the meteorological parameters of the local meteorological station; I_0 is the solar constant. The formula for calculating the solar constant at the upper bound of the Earth's atmosphere on different dates of the year is: $I_0 = 1367\left[1 + 0.033\cos(\frac{360°N}{365})\right]$, *N* is the ordinal number of days in a year starting from January 1st [10]. The empirical estimation formula for scattering intensity on a horizontal plane is:

$$I_d = I_m(1 - 1.13K_T). \quad (3)$$

In the formula, K_T is the coefficient of clear sky, which can be taken as 0.3~0.8 for cities in the latitude range of 30°~40° in China, and 0.8~1.0 for other latitude regions. There is a linear relationship between the ratio of daily average scattering and average total radiation on the horizontal plane and the clear sky coefficient [10].

The calculation formula for the intensity of reflected radiation received by a receiving surface inclined to the ground is:

$$I_f = \rho^*(I_m + I_d)(1 - \cos\beta)/2. \quad (4)$$

In the formula, ρ^* is the ground reflection coefficient, which can be taken as 0.1 for general ground and 0.2 for water surface reflection [10]. Thermal radiation simulation is defined by surface heat flux in the Abaqus load module. By applying the above radiation loads and convective loads, combined with thermal performance parameters such as thermal conductivity and specific heat capacity, and reasonably setting the predefined temperature field of the model, the simulation of the temperature field of concrete structures under sunlight can be achieved.

2 Simulation and Monitoring of Temperature Field in the Basement of Nanchang Modern Service Industry Park

2.1 Overview of Concrete Basement Structure

This chapter establishes an Abaqus refined model based on the basement of Building 8 in Nanchang Modern Service Industry Park, and uses the sunlight temperature field simulation method described in the previous section to analyze the heat transfer of the basement model. Compare the results obtained from finite element method simulation with the measured temperature field data, analyze the basic characteristics of the sunshine temperature field, and verify the rationality of the sunshine temperature field simulation theory.

Nanchang Modern Service Industrial Park is located in Honggutan District, with a total construction area of approximately 330000 square meters. The basement below Building 8 is a reinforced concrete shear wall structure basement, and a section of the basement located between the continuous expansion strip and the shrinkage post-cast strip at the southeast corner of the basement was selected as the monitoring object. The selected section is 36.1 m long from east to west and 33.5 m wide from north to south. The basement roof on the west side has a higher floor height, with structural floor heights of 4.1 m and 4.7 m respectively. The concrete strength grade is C35. The basic overview of the industrial park and the monitoring locations in the basement are shown in Figure 2.

2.2 Overview of basement temperature field monitoring system

This experiment used the DH2002 online monitoring and analysis system to collect temperature data from the JCJ100TW temperature sensor, with a collection interval of 1 second, and conducted uninterrupted temperature field monitoring for a period of 2 months. To obtain the distribution pattern of temperature field in the underground structure, a total of 28 monitoring points were set up in the monitoring area of the basement, including 10 on the roof, 9 on the side walls 1 and 2 respectively, and temperature sensors on the outer, middle, and inner layers along the thickness direction of the concrete structure were installed at measuring points 4, 5, 6, 8, 12, 15, 18, 21, 24, and 27. The temperature sensors located on the outer and inner layers are 20 mm away from the outer and inner surfaces of the concrete structure, respectively. The temperature sensor located in the middle layer is placed at half the thickness of the concrete structure, while the sensors at other measuring points are arranged in the outer concrete. The layout of the measuring points is shown in Figure 3 (a), and the thermometer is fixed to the rebars at the measuring point position using zip ties as shown in Figure 3 (b).

2.3 Analysis of Finite Element Modeling and Temperature Field Simulation Results

The basement structure of the monitoring area was poured on October 6, 2023. On October 23, partial soil backfilling was carried out on the outer side of the side walls. The east and south walls (at different heights of the basement structure) were exposed to the ground surface at a height of 1 m and 1.6 m, respectively. Select October 29 to October 31, 2023 as the temperature field simulation period, and establish an Abaqus refined finite element model as shown in Figure 4. The model is modeled using solid elements, and the material property parameters are shown in Table 1. The model mesh element type is C3D8RT eight node thermally coupled hexahedral structured element.

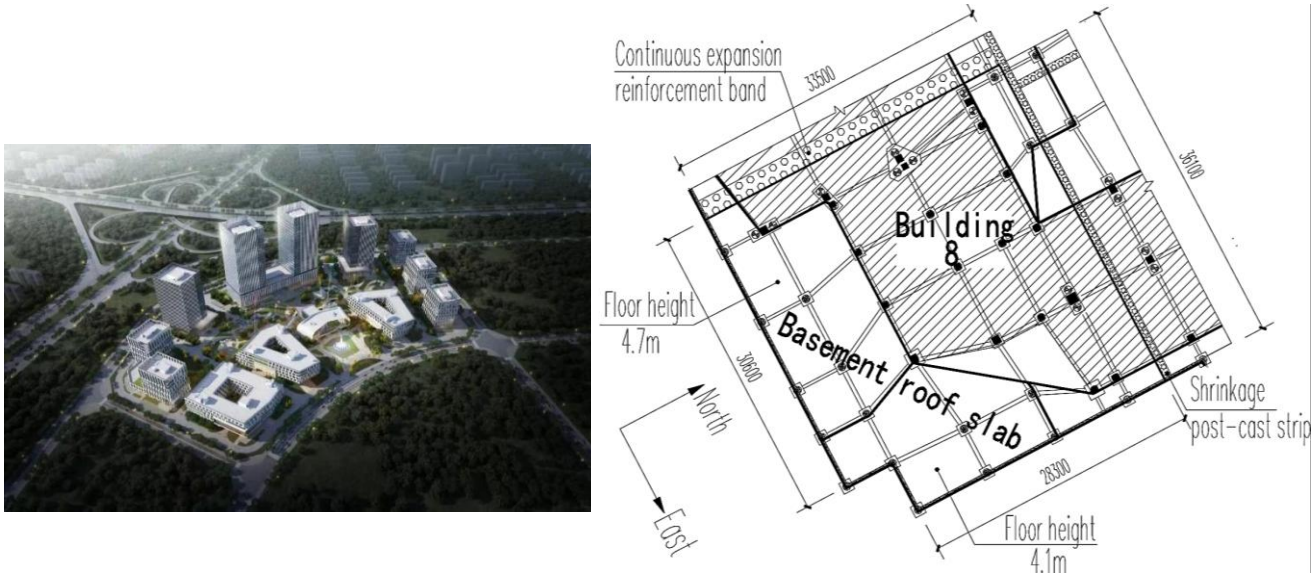

(a) Rendering of the completed park

(b) Layout plan of basement structure at monitoring location

Figure 2 – Project overview diagram

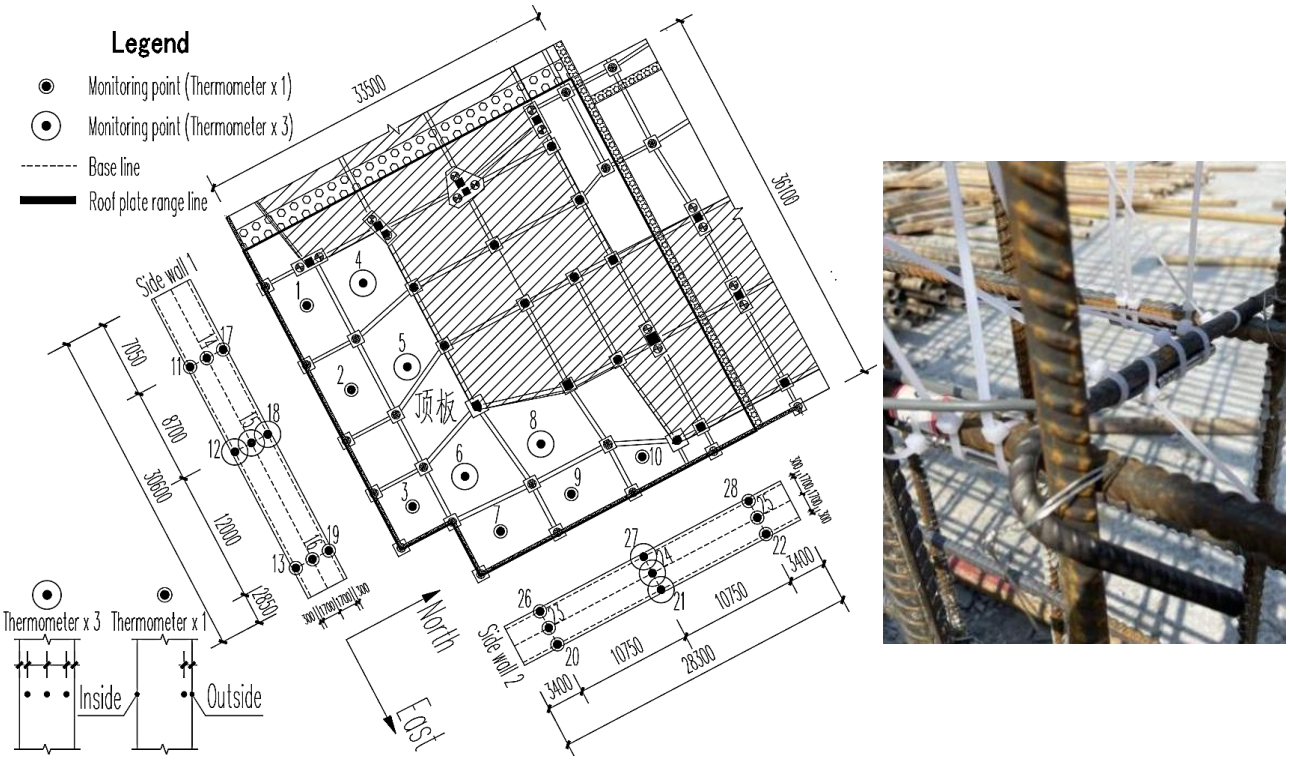

(a) Layout of basement temperature measurement points

(b) Temperature sensor binding method diagram

Figure 3 – Temperature Sensor Layout

Table 1 – Material Property Parameter Values

Property (unit: h)	Concrete grade	Density (kg/m³)	Thermal conductivity coefficient (J/h·m·°C)	Specific heat (J/kg·°C)	Thermal expansion coefficient (1/°C)	Young's modulus (GPa)	Poisson's ratio
	C35	2500	9180	930	0.00001	31.5	0.2

The atmospheric temperature data for 72 hours from October 29th to 31st, 2023 in Honggutan District, Nanchang City, obtained from the Xihe Energy Meteorological Big Data Platform, is shown in Figure 5 (a). Using the radiation load simulation theory described in the previous section, the radiation amount borne by the surface of the structure for three consecutive days was simulated, and the results are shown in Figure 5 (b) [19]. Apply heat convection and radiation load conditions to the model for heat transfer simulation analysis.

https://doi.org/10.36773/1818-1112-2024-135-3-13-23

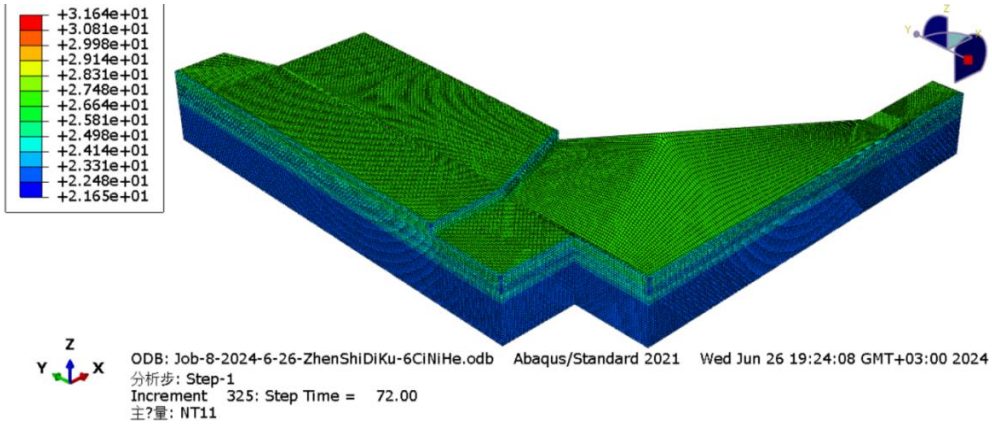

Figure 4 – Finite element model for basement heat transfer analysis (Grid size 0.15 m × 0.15 m × 0.15 m, with 65418 units; CPU: Intel (R) Core (TM) i7-8750H, 6 cores and 12 threads; System memory 8 GB, hard drive 1TB, computing time: 19 min 53 s)

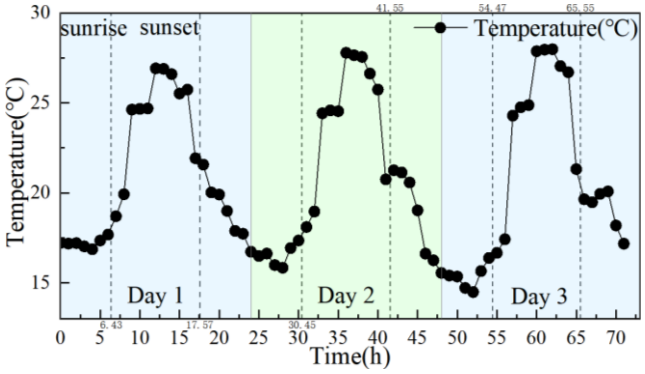

(a) Atmospheric temperature variation curve

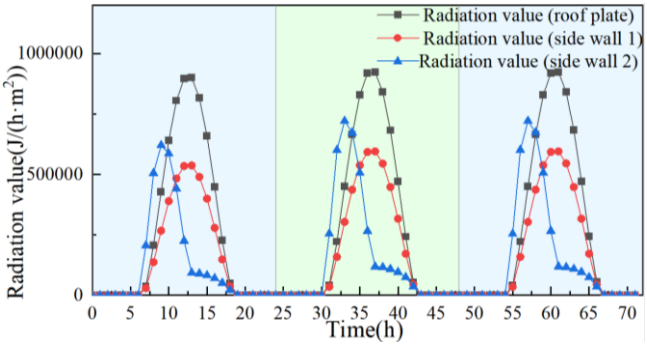

(b) Fitting curve of radiation exposure on top slab and side walls

Figure 5 – Temperature Load Simulation Data (Note: The temperature is taken from the instrument shelter located about 1.5–2 m above the ground)

Compare the temperature field simulation results with the measured data at measuring points 9, 18, 19, 28, and 4. The temperature curve comparison results are shown in Figure 6. As can be seen from the results, temperature undergoes tidal changes with sunrise and sunset. Along the thickness direction, there is a temperature gradient inside the component, and as the distance from the structure increases to the depth of the heated outer surface, the temperature change exhibits a more pronounced "hysteresis". Due to the rise and fall of the sun in the east and west, as well as the location of buildings, temperature peaks of components in different orientations alternate. The above three points are significant characteristics that distinguish the high-temperature sunlight temperature field from other temperature fields such as structural hydration heat temperature field and indoor heat source temperature field.

The temperature simulation results of the basement structure are basically consistent with the measured results. However, due to the presence of tall buildings under construction on the west side of the basement in real construction sites, as well as different levels of construction material accumulation on the basement roof, inconsistent radiation absorption intensity of various parts of concrete components, and many complex influencing factors, there are certain discrepancies between simulation results and actual measurement results. The most significant difference is that the temperature distribution of the same part (such as the outer surface) of the same component (such as the top plate) in real structures is uneven, while the finite element model results are uniform. This is due to the finite element model appropriately simplifying the model and influencing factors within a reasonable range. Overall, the error is within an acceptable range, and the temperature change trend of numerical simulation results is consistent with the measured results. The simulation theory of sunshine temperature field proposed earlier is reasonable and feasible.

3 XFEM numerical simulation analysis

3.1 Extended Finite Element Theory

To study the quantitative relationship between the length of concrete structures and the critical temperature difference for side wall cracking, it is necessary to simulate crack growth in a refined finite element model. Considering the brittle characteristics of concrete materials, the XFEM method is based on the theory of linear elastic fracture mechanics and adopts the first strength theory (maximum principal stress criterion) as the criterion for identifying concrete damage (cracking). According to equation (5), pure compressive stress (with negative σ_{max}) will not cause cracking damage, and when f reaches 1, damage (cracking) begins to trigger. Where σ_{max} is the maximum principal stress value of concrete, $\sigma^0_{\max}$ is the maximum allowable stress, and " $\langle\,\rangle$ " is the Macaulay bracket [20].

$$f = \left\{ \frac{\langle \sigma_{\max} \rangle}{\sigma^0_{\max}} \right\}. \quad (5)$$

The extended finite element method determines whether the element is damaged by setting the parameters of the traction-separation law. Set the side wall as the crack propagation area, take the maximum allowable stress as its axial tensile strength characteristic value f_{tk} = 2.2 MPa [21, 22]. According to the fracture energy results of crushed stone concrete measured by Jia Yandong et al. using the wedge splitting method, the fracture energy of concrete is approximately 150~200N/m when the compressive strength value of the concrete cube at 28 days is f_{cu} = 35 MPa. In order to fully develop cracks and highlight the characteristics of crack morphology, the fracture energy of C 35 concrete is taken as 150 N/m [23]. The analysis only considers the propagation of side wall cracks under heating conditions, and does not study the situation after the crack interface closes during the cooling process. Abaqus calculates the stress (strain) state at the center of mass of the element in front of the crack and determines whether the damage initiation criterion has been reached, thereby determining the direction of crack propagation.

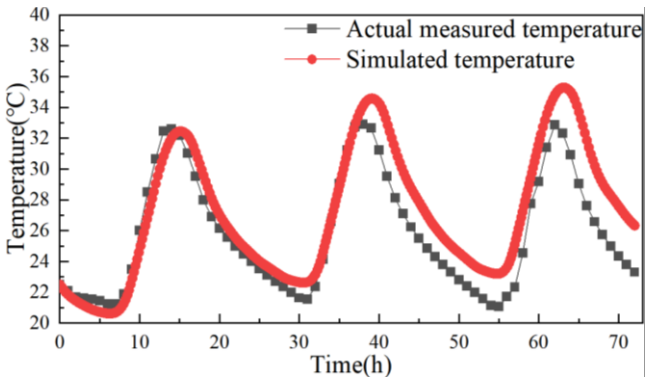

(a) Measurement point 9

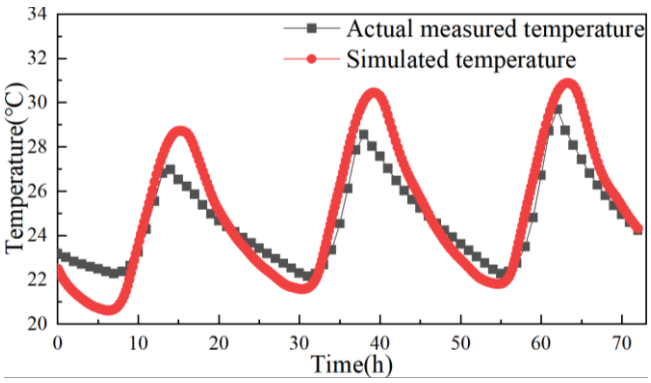

(b) Measurement point 18

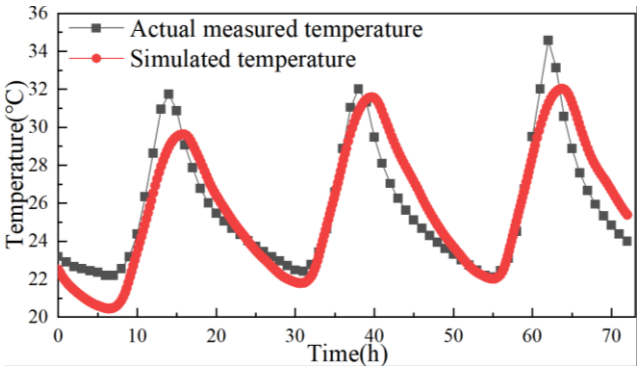

(c) Measurement point 19

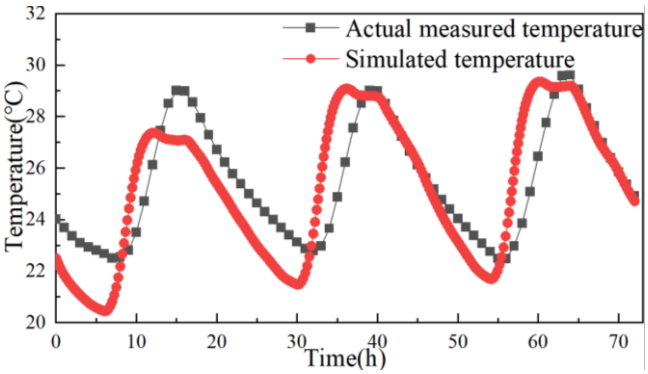

(d) Measurement point 28

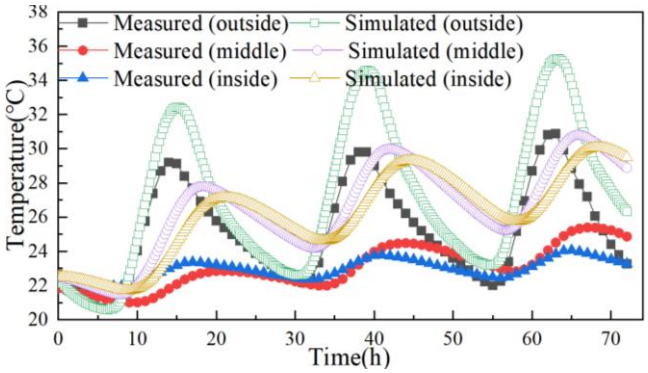

(e) Measurement point 4 (outer, middle, inner)

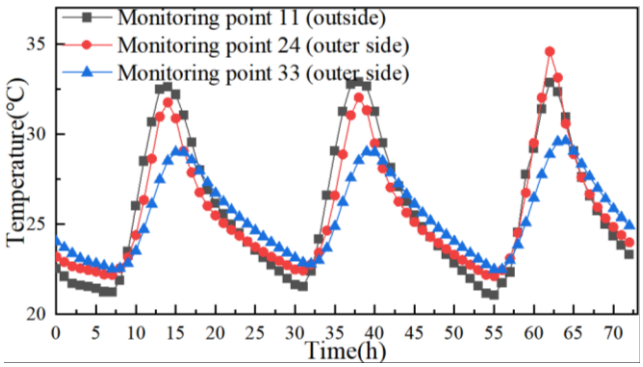

(f) Measurement points 9, 19, 18

Figure 6 – Comparison of Simulation Results of Temperature Field and Measurement Results

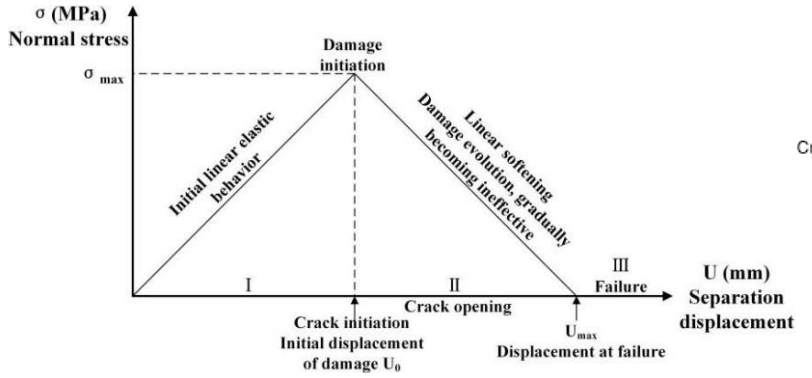

(a) Bilinear Traction-Separation Model

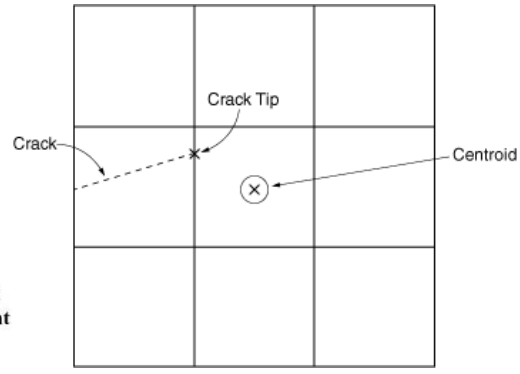

(b) Centroid and crack tip locations

Figure 7 – XFEM calculation principle

https://doi.org/10.36773/1818-1112-2024-135-3-13-23

3.2 Numerical simulation experiment

The model adopts a grillage beam floor system and an 8.1 m × 8.1 m large column grid system. The floor height is 3.9 m, the top plate is 30 cm thick, and the side walls are 30 cm thick. The bottom plate adopts a flat raft foundation with a thickness of 60 cm. Column section size: 600 mm × 600 mm, main beam section size: 900 mm × 300 mm, secondary beam section size: 600 mm × 300 mm. The rebars of the roof and side walls are arranged in an C20@200 form.

Ultra-long seamless structure refers to reinforced concrete structures where the spacing between expansion joints and post-cast strips exceeds the maximum spacing specified in the codes. According to Article 12.2.3 of the "Technical specification for concrete structures of tall building", a post construction pouring strip (joint), which connect the top plate, bottom (plate) and wall panels, can be installed every 30–40 meters in the basement of high-rise buildings [24]. Therefore, based on a 30 m basement, keeping the structural form unchanged and increasing the length of the basement, a numerical simulation experimental group was set up as shown in Table 2. To improve computational efficiency, the 1/4 modeling method is adopted for modeling. Taking the 30 m basement as an example, the refined structural model is shown in Figure 8.

Select the temperature and sunshine radiation curve of Nanchang City on August 4, 2023 as the model load, and the load curve is shown in Figure 9. To control variables, only consider the situation where the roof is affected by sunlight. Concrete and rebar modeling are respectively three-dimensional solid and solid line elements. Using a non coupled thermo-mechanical model, apply the temperature field obtained in the first step as a predefined field to the XFEM calculation file in the second step. Each experimental group's XFEM calculation file is calculated twice. The first time does not consider the cracking of the side wall and is used to calculate the stress distribution of the side wall. The second calculation simulates crack propagation to obtain the crack morphology of the side wall and the critical temperature difference between the upper and lower parts of the basement at the time of cracking.

Table 2 – Numerical Simulation Experiment Group Settings

Group.No	Model form	Length of basement (m)	Environmental temperature load
1	Plain concrete	30	Temperature and radiation curve on August 4, 2023
	With rebars		
2	Plain concrete	46.2	
	With rebars		
3	Plain concrete	62.4	
	With rebars		
4	Plain concrete	78.6	
	With rebars		
5	Plain concrete	94.8	
	With rebars		

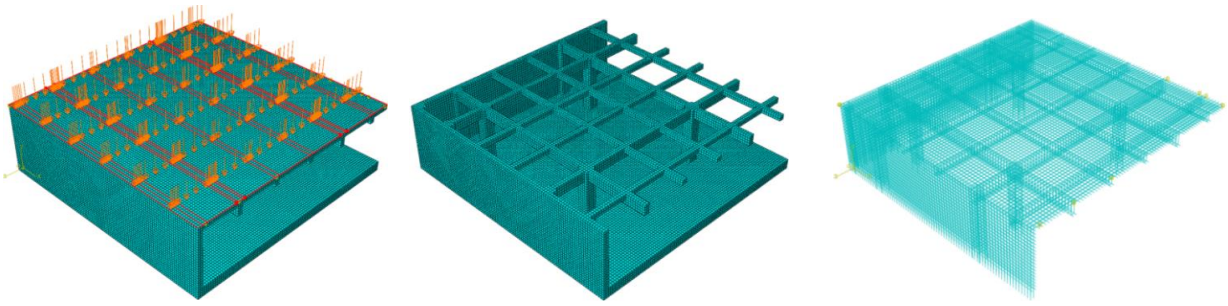

(a) Concrete structure model (b) Structural beam column system (c) Rebars model

Figure 8 – Fine grained model of 30m basement (1/4 model, with 120056 units)

In the temperature field calculation steps, the concrete and steel mesh elements are respectively an eight node linear heat transfer element (DC3D8R) and a two node heat transfer connection element (DC1D2). In the XFEM thermal stress crack calculation steps, the concrete and steel mesh elements are respectively an eight node linear hexahedral element (C3D8R) and a two node linear three-dimensional truss element (T3D2).

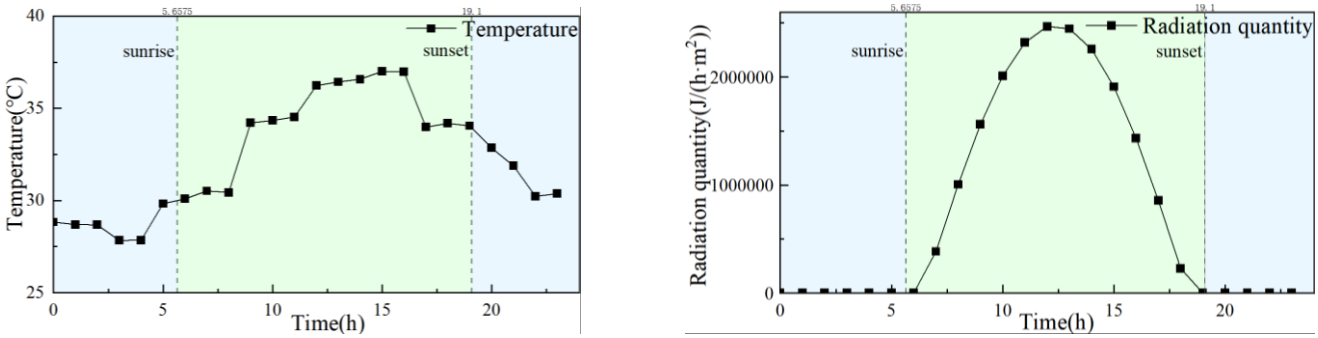

Figure 9 – Atmospheric temperature curve and sunshine radiation fitting curve in Nanchang City on August 4, 2023

3.3 Simulation result analysis

The temperature load of each experimental group is consistent, and the 24-hour temperature change curve of the top plate surface under the action of temperature changes is shown in Figure 10 (a). Analysis shows that sunlight radiation is the main factor causing significant temperature rise in the roof. For each simulation experiment, select the temperature rise range of the top plate from 30 °C to 60 °C for displacement and stress analysis.

Extract the thermal expansion deformation values of the longitudinal axis of the top plate and the top line of the side walls for each experimental group model, and plot their relationship curves with the length of the basement as shown in Figure 10 (b). According to the one-dimensional linear expansion theory, with $\Delta L = \alpha L(T_1 - T_0)$, the thermal expansion value of the material is proportional to the length L of the material, assuming that the coefficient of thermal expansion α and temperature change (T_1–T_0) remain constant. As the length of the base-

ment increases, the deviation between the maximum thermal expansion values of the central axis of the roof and the top line of the side walls and the theoretical values becomes greater. The thermal expansion values of the central axis of the 30 m reinforced concrete basement roof and the top edge of the side walls are 3.79 mm and 2.69 mm, respectively, which are 42.1 % and 29.89 % of the theoretical values; The thermal expansion values of the central axis and side wall top edge of the 94.8 m reinforced concrete basement roof are 5.74 mm and 3.41 mm, respectively, which are 20.183 % and 11.99 % of the theoretical values.

As the length of the basement increases, the number of beam and column components also increases proportionally. The large number of beam column components greatly increases the constraints on the structure, resulting in thermal expansion values far below the estimated values. Therefore, one-dimensional linear expansion theory cannot be used to estimate the magnitude of thermal expansion of basement solid structures.

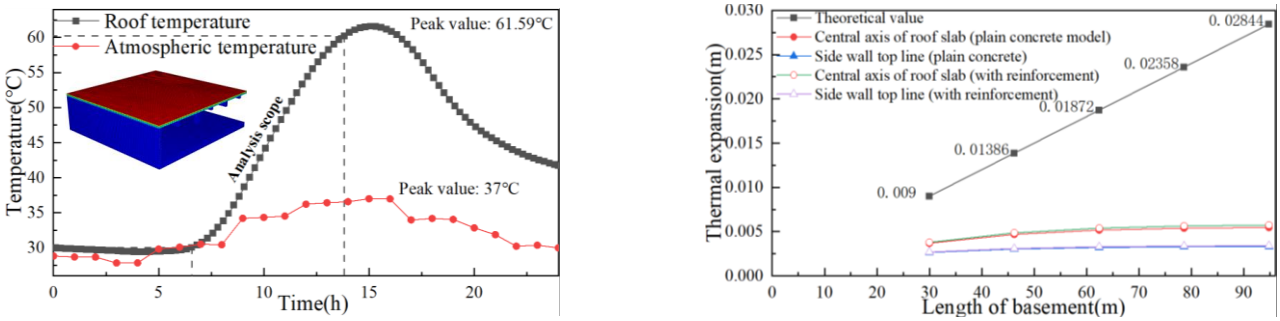

(a) Surface temperature curve on the top plate (b) Basement thermal expansion displacement curve

Figure 10 – Simulation result curve

Taking the 30 m reinforced concrete basement model as an example, as shown in Figure 11 (a), the basement roof expands in all directions with its geometric center as the expansion origin, with the maximum thermal expansion displacement at the corner of the roof. As shown in Figures 11 (b) and (c), under the effect of uneven expansion, the expansion of the basement roof is constrained by the surrounding side walls and beam column system, resulting in overall compression. The basement side walls are under overall tension, with high stress zones located at one-third on each side. The stress value is 2.2 MPa higher than the characteristic tensile strength value of C35 concrete, indicating the area where cracks develop. The reinforcing bars on the side walls are subjected to high tensile forces. As shown in Figure 11 (e), the crack propagation pattern of the side wall is an "八" – shaped diagonal crack.

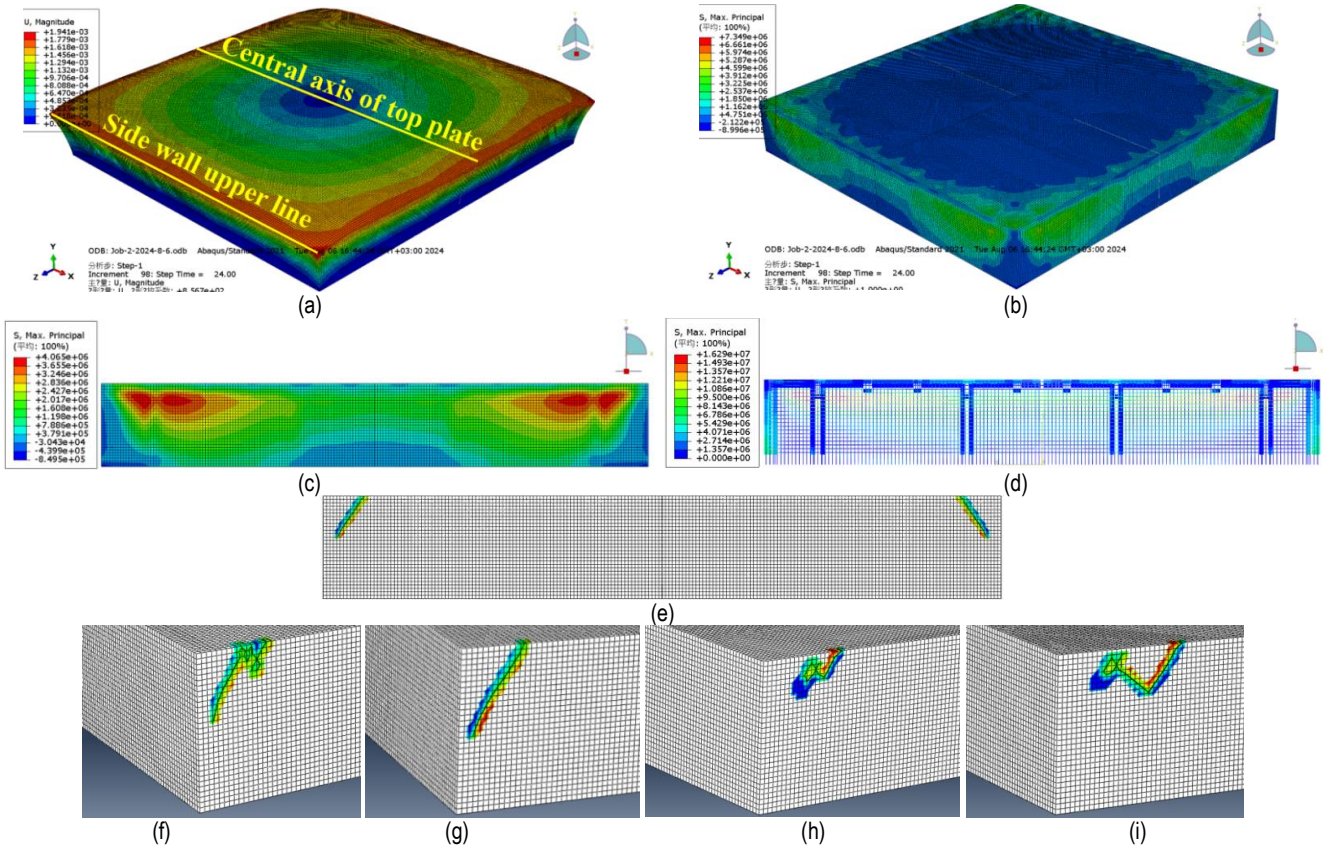

Figure 11 – Finite Element Simulation Results
(a – 30 m basement thermal expansion displacement cloud map; b – 30 m basement first principal stress cloud map; c – side wall concrete first principal stress cloud map; d – Cloud map of the first principal stress of the reinforcing steel bars on the side wall; e – Cracking result of 30 m basement side wall; f – Cracking result of 46.2 m basement side wall; g – Cracking result of 62.4 m basement side wall; h – Cracking result of 78.6 m basement side wall; i – Cracking result of 94.8 m basement side wall)

https://doi.org/10.36773/1818-1112-2024-135-3-13-23

As shown in Figure 12 (a), when the top plate is uniformly heated from 30 °C to 60 °C, the basement model increases by 216 % from 30 m to 94.8 m, while the maximum principal stress of the side walls of the plain concrete model increases by 14.656 %. The maximum principal stress of the reinforced concrete model side wall increased by 15.715 %. The increase in the length of the basement did not cause a significant increase in the side wall σ_1, the length of the basement had little effect on the stress of the side wall. In other words, reducing the stress on the side walls by significantly shortening the length of the basement is of little significance. The maximum stress value of the side walls is not significantly related to the length, and the implementation of ultra-long seamless structures is feasible.

Meanwhile, the addition of steel bars in the model not only did not reduce the stress in the concrete, but also slightly increased the stress on the side walls. This is because the thermal expansion coefficient of steel bars is larger than that of concrete, and the thermal expansion effect of the top plate after reinforcement is more severe, resulting in an increase in the stress on the side walls.

As shown in Figure 12 (b), due to the slight increase in the principal stress σ_1 of the side wall with the length of the basement, the critical temperature difference for cracking of the side wall slightly decreases. The length of the basement increased by 216 %, and the critical temperature difference for cracking decreased by 9.553 % (plain concrete) and 9.592 % (reinforced concrete), indicating that under the same temperature rise conditions, the length of the basement has a relatively small impact on the critical temperature difference for side wall cracking. The curves of the plain concrete basement and the reinforced basement basically coincide, and the addition of steel bars has no significant effect on preventing side wall cracking.

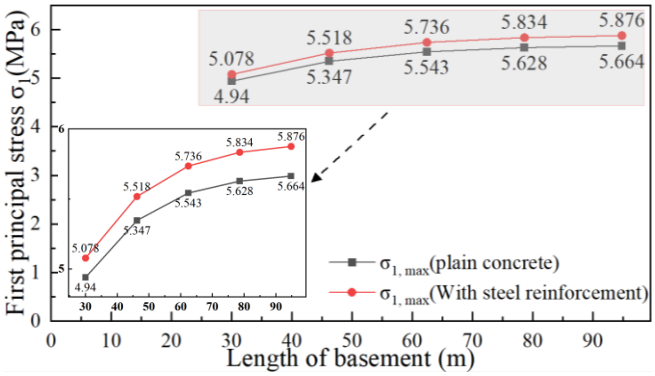

(a) Basement length-side wall first principal stress curve

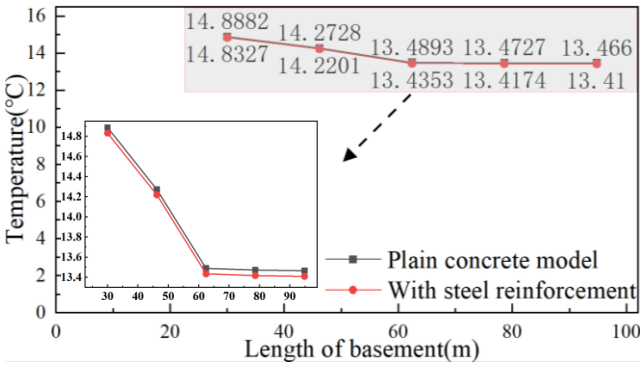

(b) Basement length-side wall cracking critical temperature difference curve

Figure 12 – Simulation result curve

4 Visualization of thermal stress trajectory in basement

The principal stress trajectory can display the load transfer path and reveal the potential direction of crack propagation. Most general finite element software currently cannot provide a complete structural stress trace diagram. Therefore, this article uses Python language to perform secondary development on Abaqus to obtain a complete principal stress trajectory diagram of the basement structure [25–28]. The idea is shown in the following Figure 13.

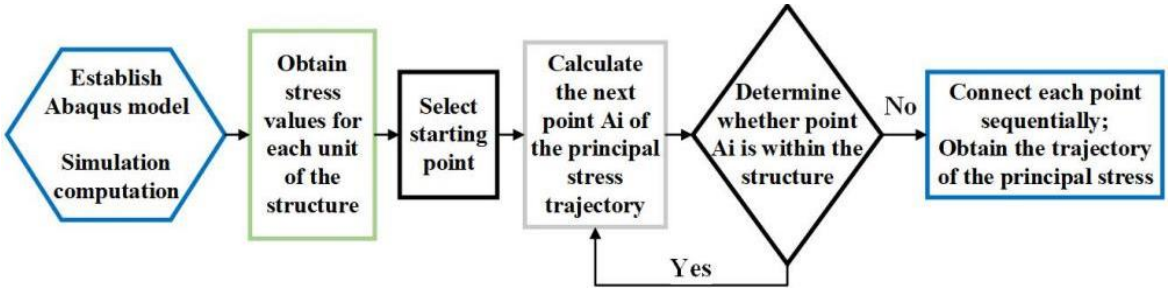

Figure 13 – Flow Chart for Automatic Drawing of Principal Stress Trajectory

The key point is to determine the direction cosine values l_i, m_i, n_i (I = 1, 2, 3) corresponding to the three principal stresses σ_i at any given point given the stress state σ_x, σ_y, σ_z, τ_{xy}, τ_{yz}, τ_{zx}. After knowing the cosine value of the direction of the point, the coordinates of the next point can be calculated based on a certain calculation step, and this process repeats itself. Solve equations (6) and (7) simultaneously. Using the cosine calculation formula of the principal stress direction provided by Wang Junbiao, the following equation is shown [29]:

$$\left.\begin{aligned}(\sigma_x-\sigma_i)l_i+\tau_{xy}m_i+\tau_{zx}n_i=0\\ \tau_{xy}l_i+(\sigma_y-\sigma_i)m_i+\tau_{yz}n_i=0\\ \tau_{zx}l_i+\tau_{yz}m_i+(\sigma_z-\sigma_i)n_i=0\end{aligned}\right\}. \quad (6)$$

$$l_i^2+m_i^2+n_i^2=1. \quad (7)$$

$$\left.\begin{aligned}l_i=\frac{A_i}{\sqrt{A_i^2+B_i^2+C_i^2}}\\ m_i=\frac{B_i}{\sqrt{A_i^2+B_i^2+C_i^2}}\\ n_i=\frac{C_i}{\sqrt{A_i^2+B_i^2+C_i^2}}\end{aligned}\right\}. \quad (8)$$

In the formula: $A_i=\tau_{xy}\tau_{yz}-(\sigma_y-\sigma_i)\tau_{zx}$;

$B_i=\tau_{xy}\tau_{zx}-(\sigma_x-\sigma_i)\tau_{yz}$;

$C_i=(\sigma_x-\sigma_i)(\sigma_y-\sigma_i)-\tau_{xy}^2$.

When the surface temperature of the basement roof is 60 °C, the stress calculation results of the 30 m basement are extracted. Taking the side wall as an example, the first principal stress trajectory is drawn as shown in the following Figure 14.

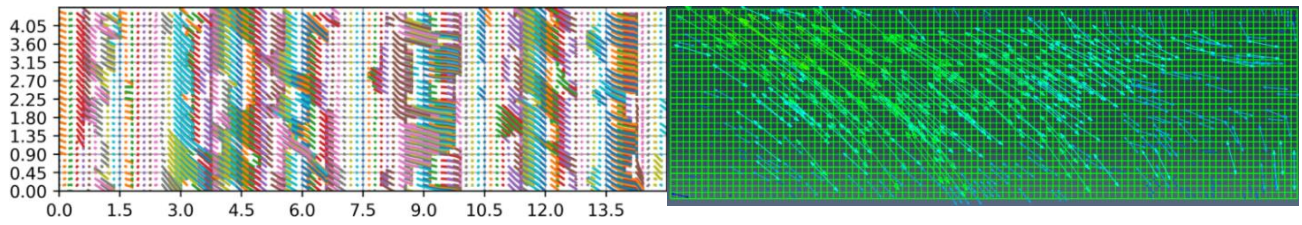

(a) Python script drawing results (b) Abaqus result principal stress vector diagram

Figure 14 – Trajectory diagram of the first principal stress on the 30 m basement side wall (1/2 side wall)

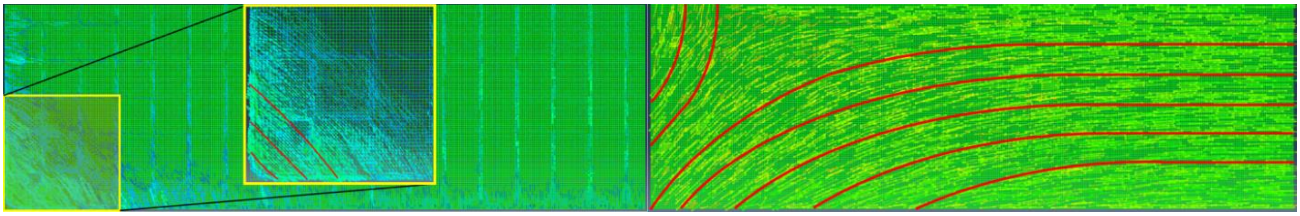

(a) First principal stress vector diagram (b) Third principal stress vector diagram

Figure 15 – Principal stress vector diagram of 94.6 m basement roof (1/4)

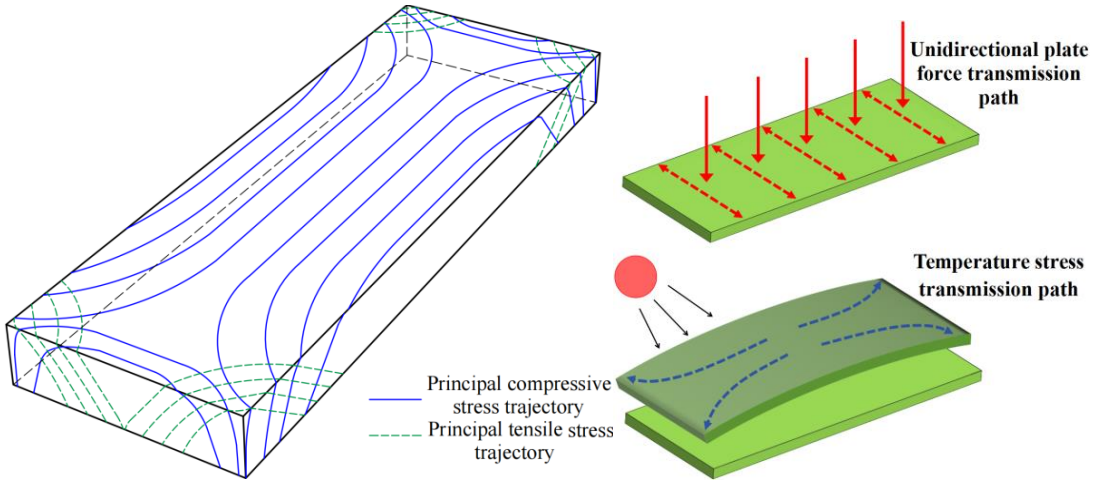

(a) Principal stress trajectory of concrete basement (b) Unidirectional plate force transmission path

Figure 16 – Schematic diagram of the transmission path of force

As can be seen from the figure, different from the general load action, temperature stress tends to propagate along the longest constrained path in the structure, that is, the "longest direction propagation" mechanism. The general load in the structure tends to be transmitted along the short direction (the path with higher stiffness), while minimizing the transmission through the path with lower stiffness as much as possible. The short stiffness of a unidirectional plate is much greater than its long stiffness, so the unidirectional plate transmits force along the short direction.

At the 1/3 positions on both ends of the longitudinal side wall, the main tensile stress traces are in the shape of "\" and "/" respectively, and this area is the high stress zone of the side wall. Therefore, cracks will develop in an "八" shape.

Conclusions

Based on the analysis of the response results of reinforced concrete basement structures with different lengths under high-temperature sunlight, the following basic conclusions can be drawn:

1. When the temperature gradient between the upper and lower parts of the basement structure is the same, increasing the length of the basement does not cause a significant increase in the principal stress values of the side walls. The ultra-long seamless structure is still reasonable and feasible under the uneven expansion effect caused by the high temperature of sunlight.

2. Under the uneven expansion effect caused by high temperature sunlight, the increase in basement length did not significantly reduce the critical cracking temperature difference value of the side walls. In engineering practice, under the same structural form, longer basement structures and shorter basement structures generally have the same temperature control range. Unlike the vertical cracks that usually appear on basement side walls, the uneven expansion effect causes the side wall cracks to form an "八" shape. This indicates that the common vertical cracks in basement side shear walls in engineering are unlikely to be caused by uneven expansion effects.

3. Unlike the stress propagation caused by general loads, the thermal stress generated by temperature action shows a trend of "longest direction propagation" in the structure, that is, temperature stress tends to propagate along the longest constrained path.

https://doi.org/10.36773/1818-1112-2024-135-3-13-23

References

1. Li Yang. Finite element simulation and temperature field analysis of super long concrete structure with expansion reinforcement [D] / Li Yang. – Hebei University of Engineering, 2021.
2. Analysis of effects on basement exterior wall cracks controlling measure [J] / Hou Juling, Peng Yunlin, Zhang Weiyang [et al.] // Construction Technology. – 2017. – Vol. 46(S2). – P. 1121–1123.
3. Treshchinostojkost' zhelezobetonnoj stenki v usloviyah stesnennoj osnovaniem temperaturnoj deformacii [J] / YU. G. Barabanshchikov, K. V. Semenov, S. S. Zimin [i dr.] // Stroitel'stvo unikal'nyh zdanij i sooruzhenij. – 2018. – № 8. – S. 51–62.
4. Wei Yinyin. Temperature effect analysis and crack control of super long concrete shear wall during construction period [D] / Wei Yinyin. – Chongqing University, 2019.
5. Zhou Ningbin. Study on early temperature stress of basement exterior wall and crack control [D] / Zhou Ningbin. – Chang'an University, 2020.
6. Yang Li. Finite element simulation and temperature field analysis of super long concrete structure with expansion reinforcement [D] / Yang Li. – Hebei University of Engineering, 2021.
7. Modelirovanie vliyaniya gradientov temperatur na raspredelenie napryazhenij na stadii gidratacii betonov / YU. A. Abzaev, A. I. Gnyrya, S. V. Korobkov [i dr.] // Vestnik Tomskogo gosudarstvennogo arhitekturno-stroitel'nogo universiteta. – 2016. – № 3 (56). – S. 129–138.
8. Chen Junyi. Analysis on temperature stress of super-long concrete structure and research on its control technology [D] / Chen Junyi. – Zhejiang University, 2006.
9. Temperature simulation and thermal effect research one extremely long-span concrete frame structure [J/OL] / Zhang Hanshuo, Bu Fanmin, Nie Jianguo [et al.] // Engineering Mechanics. – 2024. – Vol. 1–9.
10. Li Ziyi. Research on sunshine temperature field of curved concrete box girder bridge and its effects [D] / Li Ziyi. – Dalian University of Technology, 2022.
11. Xie Zhiqian. Solar Radiation Simulation Method for Hydraulic Concrete Structure [J] / Xie Zhiqiang, Fu Zhi, Lv Xingdong // Journal of Chongqing Jiaotong university(natural science). – 2019. – Vol. 38 (11). – P. 82–89.
12. Marzec, I. Quantitative assessment of the influence of tensile softening of concrete in beams under bending by numerical simulations with XFEM and cohesive cracks [J] / I. Marzec, J. Bobiński // Materials. – 2022. – Vol. 15(2). – P. 626.
13. Zhou Linren. Experimental investigation into effect of surface roughness on convective heat transfer of concrete [J] / Zhou Linren, Li Shaoji, Chen Lan // Journal of South China University of Technology (Natural Science Edition). – 2023. – Vol. 51(07). – P. 81–89.
14. Liu Xingfa. Temperature stress analysis of concrete structures [M] / Liu Xingfa. – People's Transportation Press, 1991.
15. Duffie, J. A. Solar engineering of thermal processes, photovoltaics and wind [M] / J. A. Duffie, W. A. Beckman, N. Blair. – John Wiley & Sons, 2020.
16. Liu Cheng. The temperature field and thermal effect of steel-concrete composite bridges [D] / Liu Cheng. – Tsinghua University, 2018.
17. GB 50010-2010, Code for Design of Concrete Structures (in Chinese) [S].
18. GB 50176-2016, Code for Thermal Design of Civil Buildings (in Chinese) [S].
19. Xihe Energy Meteorological Big Data Platform. Global Modeling and Assimilation Office (GMAO) (2015), MERRA-2 tavg1_2d_lnd_Nx, tavg1_2d_rad_Nx, tavg1_2d_slv_Nx: 2d,1-Hourly, Time-Averaged, Single-Level, Assimilation, Diagnostics V5.12.4 (M2T1NXSLV), Land Surface Diagnostics V5.12.4 (M2T1NXLND), Radiation Diagnostics V5.12.4 (M2T1NXRAD), Greenbelt, MD, USA, Goddard Earth Sciences Data and Information Services Center (GES DISC). – URL: https://www.xihe-energy.com (date of access: 14.09.2024).
20. Numerical Simulation of Fracture Performance of Concrete Three-Point Bending Beam Based on Extended Finite Element Method [J] / Zuo Yongmei, Guo Zhanglei, Zhu Lihua [et al.] // Journal of Hebei University of Engineering(Natural Science Edition). – 2022. – Vol. 39(04). – P. 26–32.
21. Roth, S. N. A combined XFEM–damage mechanics approach for concrete crack propagation [J] / S. N. Roth, P. Léger, A. Soulaïmani // Computer Methods in Applied Mechanics and Engineering. – 2015. – Vol. 283. – P. 923–955.
22. Liu Chun. Experimental investigation on fracture behavior of concrete under three point bending test and numerical simulation [D] / Liu Chun. – Guizhou university, 2017.
23. Jia Yandong. Research on the Fracture Performance and Experimental Methods of Concrete with Different Coarse Aggregates and Strength Grades [D] / Jia Yandong. – Dalian University of Technology, 2003.
24. JGJ 3-2010.Technical specification for concrete structures of tall building (in Chinese)[S].
25. 3D-TSV: The 3D trajectory-based stress visualizer / J. Wang, C. Neuhauser, J. Wu [et al.] // Advances in Engineering Software. – 2022. – Vol. 170. – P. 103144.
26. Yuan Yafei. Research of the method stress field's visualization based on principal stress trajectory [D] / Yuan Yafei. – Xi'an University of Science and Technology, 2019.
27. Zhang, H. Experimental Investigation on Stress Redistribution and Load-Transfer Paths of Shear Walls with Openings / H. Zhang, X. Liu, W. Yi // Journal of Structural Engineering. – 2018. – Vol. 144(9). – P. 296–311.
28. Kelly, D. W. An algorithm for defining load paths and a load bearing topology in finite element analysis / D. W. Kelly, C. A. Reidsema, M. C. W. Lee // Engineering Computations. – 2011. – Vol. 28(2). – P. 196–214.
29. Wang Junbiao. Formula for calculating the principal direction of stress[J] / Wang Junbiao // Mechanics in Engineering. – 1992. – Vol. 04. – P. 60.

Material received 18/09/2024, approved 19/11/2024, accepted for publication 19/11/2024